CrystEngComm

Accepted Manuscript

ROYAL SOCIETY OF CHEMISTRY

www.rsc.org/crystengcomm

Facile Synthesis of Cu-Ag Hybrid Nanowires with Strong Surface-enhanced Raman Scattering Sensitivity

Zhi Jiang, Yanhong Tian*, Su Ding, Jiayue Wen, Chenxi Wang

State Key Laboratory of Advanced Welding and Joining, Harbin Institute of Technology, Harbin, China, 150001.

E-mail address: tianyh@hit.edu.cn

Abstract:

Cu-Ag hybrid nanowires with well-defined Ag nanoparticles on the surfaces of Cu NWs were successfully prepared by a mild two-step method. High resolution transmission electron microscope (HRTEM) results indicated that as-prepared silver nanoparticles (Ag NPs) with an average diameter of 8.4 nm were directly grown on the surfaces of copper nanowires (Cu NWs) through an in situ substitutional reaction with Cu-Ag metallic bonds forming between Ag NPs and Cu NWs. Growth evolution results showed that Ag nanoseeds were prone to grow into Ag NPs when the ratio of Cu to Ag was small while they tended to grow into Ag nanowires (NWs) as the ratio of Cu to Ag dramatically increased. Furthermore, the strong surface-enhanced raman scattering sensitivity (SERS) effect of as-prepared Cu-Ag hybrid NWs was verified using Rhodamine 6G (R6G) and 4-aminothiophenol (4-ATP) probes.

Introduction:

SERS phenomenon has been attracting active attention in recent decades because Raman signals of non-resonant molecules could be enhanced by significant orders of magnitude when these molecules were adsorbed on well-defined noble metallic nanostructures [1-4]. Typically, size, shape, and crystallinity of nanomaterials, as well as geometric construction between nanostructures could greatly affect the intensity of Raman signals [5]. For instance, strongly coupled Ag NPs have already been reported to generate dramatically amplified electromagnetic field between coupled NPs in the tiny gap region (usually called as "hot spot"), which would greatly improve detection accuracy with enhanced Raman signals [6]. Several methods have been reported to achieve a precise control over the configurations of NPs, such as self-assembly, oblique angle vapor deposition, templates as well as nanolithography method [7-10]. However, the precise manipulation of nanoscaled components requires expensive equipment and the operation process is extremely complex in these methods.

Recently, simple solution process was developed to fabricate Ag NPs-attached surfaces, which was believed to be a most promising alternative method [11]. Well-arrayed Ag NPs were attached on various materials, such as silicon NWs, graphene, carbon nanotubes, nanofibrous membranes, Cu_2O NWs, and $ZnGa_2O_4$ nanorods [12-19], and they could provide numerous hot spots in the gap areas. However, organic coating layer, existing between Ag NPs themselves as well as Ag NPs and supportive nonmetallic materials, could greatly damage the magnifying effect of coupled Ag NPs on Raman signals due to uncertainties in regard to

improving the efficiency of charge separation and transport, and they are usually unremovable without leading to significant changes on the size and morphology of nanostructures [20-22]. Ag layer has already been reported to be prepared on the surfaces of Cu nanomaterials to form Cu@Ag core-shell nanomaterials using chemical plating method in aqueous solution without organic layer between Ag layer and Cu nanomaterials [23-26]. Also, the cost of this simple solution method is greatly lowered down due to the cheap raw materials as well as scalable process, which is suitable for large scale production. Thus, Cu-Ag hybrid nanowires with well-defined Ag nanoparticles on the surfaces of Cu NWs was expected to be fabricated by this simple solution method, and generate strong SERS sensitivity [27].

Here we report a facile method to directly develop well-arrayed Ag NPs on Cu NWs through in situ reducing of Ag^+ ions in aqueous solution without any addictive foreign reducing agent or stabilizing agent. The morphology of as-prepared Cu-Ag hybrid nanowires could be controlled by adjusting reactive parameter, such as time and ratio of Cu to Ag, and the mechanism and regularity of the growth of Cu-Ag hybrid nanowires were analyzed. Also, the detecting of typical organic molecules using as-prepared Cu-Ag hybrid nanowires was conducted in this work.

Experimental

Analytical grade salt copper dechloride ($CuCl_2 \cdot 2H_2O$), silver nitrate ($AgNO_3 \cdot H_2O$), hexadecylamine (HDA), ammonium hydroxide ($NH_3 \cdot H_2O$), sulphuric acid (H_2SO_4) and glucose were used as received without further purification.

Synthesis of Cu-Ag hybrid NWs: Cu-Ag hybrid NWs were prepared by a mild two step method. In the first step, the Cu NWs were synthesized by a method in our previous paper and they were dispersed in 10 mL water for use [28]. In the second step, ammonium hydroxide was added into $AgNO_3$ (0.1 mM) solution by dropping until colorless transparent plating solution was obtained. Then add the obtained solution into Cu NWs (1 mM) solution by dropping under vigorous stirring. The solution quickly changed into black from deep purple, indicating the formation of Ag NPs. After kept for 10 minutes, the resulting solution was centrifuged and washed with water and ethanol in turn for three times. The product was conserved in ethanol.

Fabrication of the simple SERS biodetection platform: one piece of silicon was coated by a layer containing the hybrid nanostructures and the other piece of silicon had no special treatment, and then R6G aqueous solution or 4-ATP ethanol solution was dropped onto these two pieces of silicon substrates.

Characterization of the morphology and property: X-ray Diffraction (XRD) pattern was collected with a Rigaku D/max-γB diffractor meter with Cu K_α irradiation. X-ray photoelectron spectroscopy (XPS) data was obtained using a monochromatic Al K_α source. Morphology and structure of the NWs were checked with a field-emission SEM (FEI Quanta 200F) and a FEI Tecnai G^2 F30 microscope operated at 300 kV. TEM samples were prepared by transferring a drop of dispersed solution containing powders to a holey carbon film supported on Cu grid. The SERS spectra were recorded with a microscopic confocal Raman spectrometer, using a laser beam with an excitation wavelength of 633 nm and a charge-coupled device (CCD) detector.

Results & discussion

The morphology and phase composition changes after the coating of Ag NPs on the surfaces of Cu NWs were characterized by TEM images and XRD results. Figure 1a shows the morphology of as-prepared Cu NWs with diameter around 40 nm and length up to tens of micrometers. Before coating, the surfaces of Cu NWs were extremely smooth and covered with organic residues. The XRD result in figure 1c shows that there are three peaks at 2θ =43.3, 50.4, and 74.1°, corresponding to the diffractions of the {111}, {200}, and {220} crystal planes of face-centered cubic (fcc) Cu (JCPDS 04-0836), respectively [28]. After substitutional reaction, the surfaces of NWs became coarse due to well-arrayed NPs attached on the surfaces of Cu NWs as shown in figure 1b, and also organic residues disappeared probably as the result of further cleaning. The XRD result of the hybrid structures in figure 1c demonstrates that there are three other peaks apart from those belonging to Cu. One of clearly identifiable peaks is the one at 2θ=38.1°, corresponding to {111} crystal planes of face centered cubic (fcc) Ag (PDF 65-2871). Besides, there are two relatively weaker diffraction peaks at 2θ=64.4 and 77.4°, which correspond to {220} and {311} crystal planes, respectively. Also, one of main peaks of Ag at 2θ=44.3° could not be identified due to overlapping with the main peak of Cu. The above description indicates that well-arrayed Ag NPs were grown on the surfaces of Cu NWs by this simple solution method.

XPS analysis was further conducted to thoroughly investigate the element composition of Cu-Ag hybrid NWs. Figure 2 shows XPS data comparison between

Cu NWs and Cu-Ag hybrid NWs. Survey spectra in figure 2a illustrated that Cu and Ag elements coexisted in Cu-Ag hybrid NWs while Cu NWs did not contain any Ag element, which could confirm that Ag NPs was generated on the surfaces of Cu NWs after the substitutional reaction. $Cu2p_{3/2}$ and Ag3d peaks were further compared in figure 2b and 2c. In figure 2b, the peak position of $Cu2p_{3/2}$ of Cu-Ag NWs was at the same position as that of Cu NWs, i.e. at binding energy equaling to 923.3 eV, while the peak intensity of $Cu2p_{3/2}$ of Cu-Ag NWs was much greater than that of Cu NWs, which could be resulted from different sample-making process [29]. Figure 2c clearly demonstrated that binding energies of $Ag3d_{5/2}$ and $Ag3d_{3/2}$ electrons were 374.25 eV and 368.15 eV, respectively. Silver usually exists in three different states, i.e. AgO state with energy of 367.0 eV, Ag_2O state with energy of 367.7 eV, and Ag^0 state with energy of 368.2 eV as reported before [30]. Comparing these values, it is clear that Ag mainly existed in Ag^0 state, and in other words Ag NPs were successfully prepared on the surfaces of Cu NWs in Ag^0 state.

The structure of as-prepared Cu-Ag hybrid NWs is further characterized by TEM. In figure 3a, TEM image for the hybrid structures shows that the surfaces of Cu NWs are totally covered by the tiny-sized Ag NPs. These Ag NPs are of about 8.4 nm as calculated from 100 NPs on 10 Cu NWs. The SAED result in figure 3b demonstrates there exists three sets of diffraction spots. Two sets of diffraction spots with share spots belong to Cu NWs with a twined-structure, and they correspond to the [001] and [112] zone axis, respectively, which has also been reported in our recent paper and others [28, 31-33]. Another set of diffraction spots belongs to Ag NPs, corresponding

to the [111] zone axis. The remaining spots originate from the generation of double diffraction, which is induced by the mutual orientation of these three zones [34]. It is worthy to mention that the crystal orientation of Ag [-220] was the same with that of Cu [-220], indicating the {220} facets of Ag NPs and Cu NWs were grown in the same direction. Figure 3c shows the HR-TEM image of the interface between Cu NW and Ag NP. The interplanar spacing of 0.2068 nm corresponds to (111) plane of Cu NWs, while that of 0.2411 nm corresponds to (111) plane of Ag NPs, and the angle between these two facets was only 8.5°. The configuration of Cu NW and Ag NP was estimated as shown in figure 3d. On the other hand, moire fringe with width of 0.4971 nm was generated due to the overlapping of Ag and Cu atoms mentioned above. The width of moire fringe and the interplanar spacing of overlapping atoms satisfy the following equations [35]:

$$\sin\psi = \frac{d_1 d_2 \sin\theta}{\sqrt{d_1^2 + d_2^2 - 2d_1^2 d_2^2 \cos\theta}} \quad (1)$$

$$\cos\theta = \frac{(d_1^2 + d_2^2)\mathrm{d}_m^2 - d_1^2 d_2^2}{2\,\mathrm{d}_m^2\, d_1 d_2} \quad (2)$$

Where ψ is the angle between lattice fringe of (111) plane of Cu NWs and moire fringe, θ is the angle between lattice fringe of (111) plane of Cu NW and that of (111) plane of Ag NP, d_1 and d_2 are the width of lattice fringe of (111) plane of Cu NW, and Ag NP, respectively, and d_m is the width of moire fringe. Besides, the tight interface indicates the nonexistence of any organic surfactant and the formation of Cu-Ag metallic bonds between Ag NPs and Cu NWs after substitutional reaction.

In order to investigate the growth regularity of Ag NPs, the standard solution was

kept for 1, 5, and 10 minutes before washed, and the corresponding SEM images were shown in figure 4a-4c. Ag NPs were relatively small when the reaction only prolonged for 1 minutes, and they gradually grew up with a mild speed. After 10 minutes, the CuNWs were covered with tiny Ag NPs around 8.4 nm as analyzed above (Figure 4c). During this process, Ag nano seeds firstly generated on the surfaces of Cu NWs and then grew bigger and bigger as more atoms gathered around. The whole process could be describe as the process I in figure 6. To investigate the influence of the amount of Ag+ ions on the morphology of Cu-Ag hybrid NWs, the concentration of Ag^+ ions was firstly doubled in the standard recipe and kept for 1, 5, and 10 minutes before washed, and the evolution process was shown in figure 4d-4f. Clearly, the surfaces of Cu NWs became coarse after the reaction was kept only for 1 min indicating fast generation of Ag seeds, which would also grow much bigger at a rate faster than that in the standard solution. When the solution was kept for 10 min, the size of the Ag NPs were much larger due to the higher concentration of Ag ions in the solution (Figure 4f).

When the concentration of Ag+ ions was ten times higher than that of standard solution, the morphology of Ag nanostructures changed greatly as shown in Figure 5. At the initial stage, Ag NPs appeared on the surfaces of Cu NWs as previous experiments. Then Ag NPs grew into longer nanorods when the reaction was kept for 5 min, and continued growing into Ag nanorods when the reaction lasted for 10 min. The whole process could be described as the process II in figure 6. It is worthy to mention that the phenomenon, i.e. Ag nanorods formed when the ratio of Cu to Ag

equals 1:1, also could be the evidence that the tiny-sized Ag NPs were well arrayed on the surfaces of Cu NWs when the Ag^+ was in the standard recipe.

The growth process of Ag nanostructure on the surfaces of Cu NWs could be described as shown in figure 5. The substitutional reaction could be estimated as the following equations [36]:

$$2AgNO_3+2NH_4OH \rightarrow Ag_2O\downarrow+H_2O+2NH_4NO_3 \quad (3)$$

$$Ag_2O+4NH_4OH \rightarrow 2[Ag(NH_3)_2]OH+3H_2O \quad (4)$$

$$[Ag(NH_3)_2]OH+NH_4NO_3 \rightarrow [Ag(NH_3)_2]NO_3+NH_4OH \quad (5)$$

$$2[Ag(NH_3)_2]NO_3+Cu \rightarrow [Cu(NH_3)_4](NO_3)_2+2Ag\downarrow \quad (6)$$

In the initial plating solution, Ag^+ ions existed as $[Ag(NH_3)_2]NO_3$ for they have a stable coordination structure and could react with Cu atoms. After the mixing of plating solution and aqueous solution of Cu NWs, Ag atom clusters will be firstly precipitated on the surfaces of Cu NWs with Ag^+ ions reduced by Cu atoms to lower down the overall chemical potential of the solution system, and these clusters act as seeds for Ag nanostructures. As {111} facets of Cu and Ag face-centered cubic crystal own the lowest surface energy, interface, instead of mixing of Cu and Ag atoms, between Cu NWs and newly-generated Ag seeds would appear and keep stable throughout the growth process of Ag nanostructures [37] . Also, these newly-formed Ag atom clusters tend to distribute randomly on the Cu NWs and are connected to Cu NWs by Cu-Ag metallic bonds. As the reaction continued in the solution, more Ag atoms could be absorbed onto the surfaces of the seeds, and seeds grew up into nanoparticles. When the ratio of Cu to Ag was larger and reaction time was shorter,

well-arrayed Ag nanoperticles formed on the surfaces of Cu NWs. As the concentration of Ag^{+} irons dramatically increased, Ag nano seeds could grow into Ag nanorods when the reaction was maintained for longer time. The morphology of the product could be well controlled by adjusting the reaction parameters and the growth mechanism of Ag nanorods is similar with that of typical Vapor-Liquid-Solid (VLS) NW growth [38].

A simple SERS biodetection platform was fabricated using the as-prepared Cu-Ag hybrid NWs to test their SERS sensitivity and two different molecules, i.e. R6G and 4ATP, were chosen as probes. Figure 7 shows the Raman spectra of R6G on bare silicon substrate and silicon substrate covered by Cu NWs and Cu-Ag hybrid NWs (Figure S3 illustrates the Raman spectra of 4-ATP with a series of concentration). Clearly, the Raman spectra gathered from bare substrate and silicon substrate covered by Cu NWs showed no obvious signal due to the low concentration of R6G molecules. In contrast, the existence of R6G molecules could be identified when the silicon substrate was covered with a layer consisting of Cu-Ag hybrid NWs, and the concentration of R6G molecules could be as low as 10^{-8} mol·L^{-1}. There were six peaks that could be identified, corresponding to 1312, 1363, 1507, 1579, 1601, and 1650 cm^{-1}, all of which belongs to the standard Raman spectra of R6G molecules [39-40]. The values of enhancement factor (EF) for R6G and 4-ATP probes was calculated to be 1.6×10^{5} and 4.5×10^{6}, respectively, the details of which were shown in supporting information. The strong SERS sensitivity should be the result of the well-coupled and well-arrayed Ag NPs on Cu NWs. As mentioned before, noble metallic nanostructures

could amplify the Raman signals of non-resonant molecules by significant magnitudes at so-called hot spots [5]. As Ag NPs were well-arrayed and well-coupled on Cu NWs, the hybrid structure itself could provide numerous hot spots at the tiny gap area of Ag NPs, where electromagnetic field would be dramatically amplified.

Conclusions:

This paper has successfully developed Cu-Ag hybrid nanowires with well-defined Ag nanoparticles on the surfaces of Cu NWs using a mild two-step method. Ag NPs were grown on Cu NWs through an in situ substitutional reaction and there existed a coherent orientation relationship at the interface between Ag NPs and Cu NWs. It is concluded that initial Ag nano seeds tended to grow up as Ag NPs when the ratio of Cu to Ag was small while they were prone to grow up into Ag nanorods when the ratio of Cu to Ag was 10 times more than the standard recipe. Moreover, a simple SERS biodetection platform was fabricated to demonstrate the strong SERS effect of as-synthesized Cu-Ag hybrid NWs by identifying the existence of R6G and 4-ATP probes in extremely low concentration.

Acknowledgment:

The authors are grateful for financial support from the National Natural Science Foundation of China (Grant No. 51522503) and support from Program for New Century Excellent Talents in University (NCET-13-0175).

Reference:

1. H. Liang, Z. Li, W. Wang, Y. Wu and H. Xu, *Advanced Materials*, 2009, **21**, 4614-4618.
2. Y. Lu, G. L. Liu and L. P. Lee, *Nano letters*, 2005, **5**, 5-9.
3. M. Fan, G. F. S. Andrade and A. G. Brolo, *Analytica Chimica Acta*, 2011, **693**, 7-25.
4. J. Zheng, Y. Zhou, X. Li, Y. Ji, T. Lu and R. Gu, *Langmuir*, 2003, **19**, 632-636.
5. W. Li, P. H. C. Camargo, X. Lu and Y. Xia, *Nano letters*, 2008, **9**, 485-490.
6. J. Zhang, X. Li, X. Sun and Y. Li, *The Journal of Physical Chemistry B*, 2005, **109**, 12544-12548.
7. A. M. Michaels, J. Jiang and L. Brus, *The Journal of Physical Chemistry B*, 2000, **104**, 11965-11971.
8. S. B. Chaney, S. Shanmukh, R. A. Dluhy and Y. P. Zhao, *Applied Physics Letters*, 2005, **87**, 031908.
9. S. J. Lee, A. R. Morrill and M. Moskovits, *Journal of the American Chemical Society*, 2006, **128**, 2200-2201.
10. M. L. Coluccio, G. Das, F. Mecarini, F. Gentile, A. Pujia, L. Bava, R. Tallerico, P. Candeloro, C. Liberale, F. De Angelis and E. Di Fabrizio, *Microelectronic Engineering*, 2009, **86**, 1085-1088.
11. J. He, T. Kunitake and A. Nakao, *Chemistry of Materials*, 2003, **15**, 4401-4406.
12. J. Yin, X. Qi, L. Yang, G. Hao, J. Li and J. Zhong, *Electrochimica Acta*, 2011, **56**, 3884-3889.
13. S. Sun and P. Wu, *Physical Chemistry Chemical Physics*, 2011, **13**, 21116-21120.
14. L. Zhang, X. Gong, Y. Bao, Y. Zhao, M. Xi, C. Jiang and H. Fong, *Langmuir*, 2012, **28**, 14433-14440.

15. A. B. Castle, E. Gracia-Espino, C. Nieto-Delgado, H. Terrones, M. Terrones and S. Hussain, *ACS nano*, 2011, **5**, 2458-2466.

16. L. Chen, M. Wu, Q. Jing, Y. Yu, J. Huang, Y. Liu, X. Liu and G. Qiu, *RSC Advances*, 2015, **5**, 67134-67140.

17. Y. Pan, S. Deng, L. Polavarapu, N. Gao, P. Yuan, C. H. Sow, and Q. Xu, *Langmuir*, 2012, **28**, 12304-12310.

18. L. Chen, J. M. Chabu, R. Jin and J. Xiao, *RSC Advances*, 2013, **3**, 26102-26109.

19. L. Chen, D. Jiang, X. Liu and G. Qiu, *CHEMPHYSCHEM*, 2014, **15**, 1624-1631.

20. G. Xi, J. Ye, Q. Ma, N. Su, H. Bai and C. Wang, *Journal of the American Chemical Society*, 2012, **134**, 6508-6511.

21. J. A. Lopez-Sanchez, N. Dimitratos, C. Hammond, G. L. Brett, L. Kesavan, S. White, P. Miedziak, R. Tiruvalam, R. L. Jenkins, A. F. Carley, D. Knight, C. J. Kiely and G. J. Hutchings, *Nature Chemistry*, 2011, **3**, 551-556.

22. L. Menard, F. Xu, R. Nuzzo and J. Yang, *Journal of Catalysis*, 2006, **243**, 64-73.

23. J. Zhang, Y. Yuan, X. Xu, X. Wang and X. Yang, *ACS Applied Materials & Interfaces*, 2011, **3**, 4092-4100.

24. M. Tchaplyguine, T. Andersson, C. Zhang and O. Bjorneholm, *The Journal of Chemical Physics*, 2013, **138**, 104303.

25. M. Tsuji, S. Hikino, Y. Sano and M. Horigome, *Chemistry Letters*, 2009, **38**, 518-519.

26. M. Tsuji, S. Hikino, R. Tanabe, M. Matsunaga and Y. Sano, *CrystEngComm*, 2010, **12**, 3900-3908.

27. H. Wang, D. W. Brandl, F. Le, P. Nordlander and N. J. Halas, *Nano letters*, 2006, **6**, 827-832.

28. Z. Jiang, Y. Tian and S. Ding, *Materials Letters*, 2014, **136**, 310-313.

29. I. Lopez-Salido, D. C. Lim and Y. D. Kim, *Surface science*, 2005, **588**, 6-18.

30. W. Su, S. S. Wei, S. Q. Hu and J. X. Tang, *Journal of hazardous materials*, 2009, **172**, 716-720.

31. S. Ding, J. Jiu, Y. Tian, T. Sugaharab, S. Nagaob and K. Suganuma, *Physical Chemistry Chemical Physics*, 2015, **17**, 31110-31116.

32. C. J. Johnson, E. Dujardin, S. A. Davis, C. J. Murphy and S. Mann, *Journal of Materials Chemistry*, 2002, **12**, 1765-1770.

33. I. Lisiecki, A. Filankembo, H. Sack-Kongehl, K. Weiss, M. P. Pileni, and J. Urban, *Physical Review B*, 2000, **61**, 4968.

34. Y. Sun, B. Mayers, T. Herricks and Y. Xia, *Nano Letters*, 2003, **3**, 955-960.

35. P. S. Theocaris and F. P. Chiang, *Journal of Applied Mechanics*, 1974, **41**, 1148.

36. X. Luo, G. A. Gelves, U. Sundararaj and J. L. Luo, *The Canadian Journal of Chemical Engineering*, 2013, **91**, 630-637.

37. R. Ferrando, J. Jellinek and R. L. Johnston, *Chemical reviews*, 2008, **108**, 845-910.

38. Y. Wu and P. Yang, *Journal of the American Chemical Society*, 2001, **123**, 3165-3166.

39. Y. Li, X. Zhao, P. Zhang, J. Ning, J. Li, Z. Su and G. Wei, *Journal of Materials Chemistry C*, 2015, **3**, 4126-4133.

40. P. Zhang, Y. Huang, X. Lu, S. Zhang, J. Li, G. Wei and Z. Su, *Langmuir*, 2014, **30**, 8980-8989.

41. L. Wang, H. Li, J. Tian and X. Sun. Monodisperse, *ACS applied materials & interfaces*, 20140, 2, 2987-2991.

Figures:

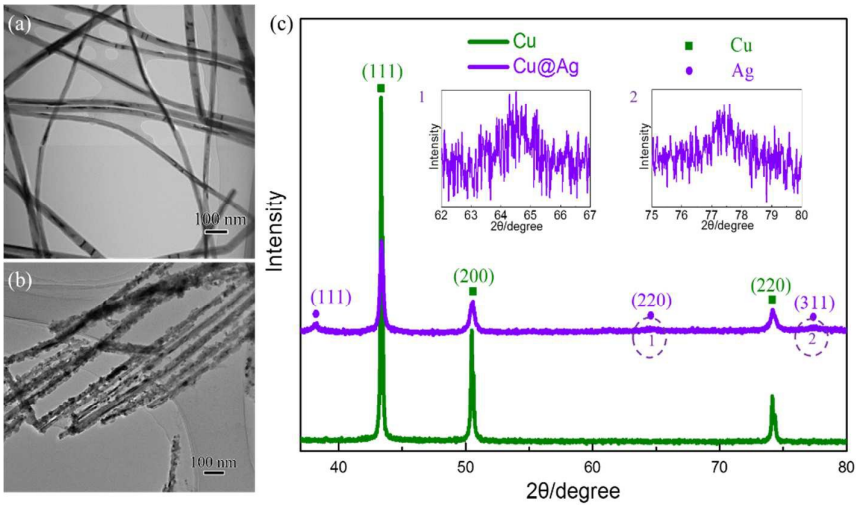

Figure 1 Morphology and phase composition changes before and after the coating of Ag NPs on Cu NWs: (a) TEM image of Cu NWs before coating (b) TEM image of Cu-Ag hybrid NWs after coating (c) XRD results of the Cu NWs and Cu-Ag hybrid NWs.

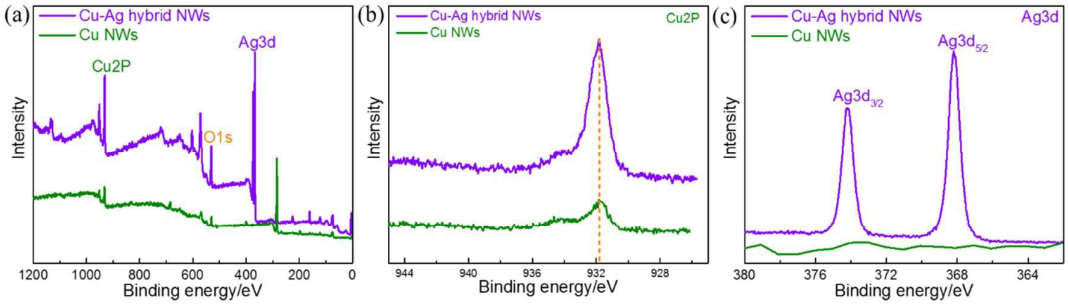

Figure 2 XPS analysis comparison between Cu NWs and Cu-Ag hybrid NWs: (a) survey spectra (b) $Cu2p_{3/2}$ spectra (c) Ag3d spectra

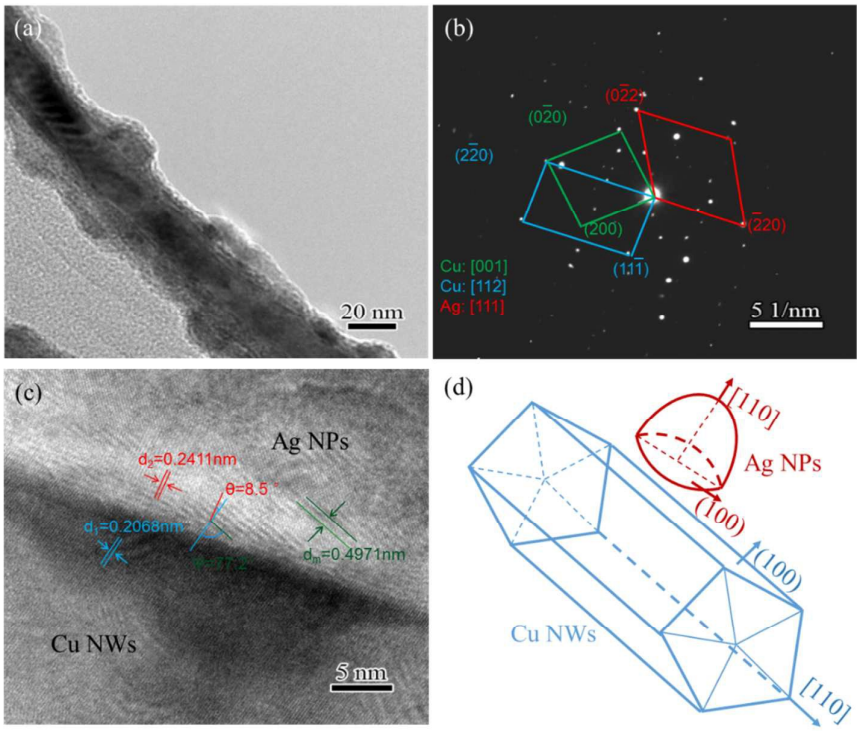

Figure 3 Structure characterization of Cu-Ag hybrid NWs: (a) TEM image of single Cu-Ag hybrid NW (b) Selective Area Electron Diffraction (SAED) results (c) HRTEM image of the interface between the Cu NW and the Ag NP (d) Scheme of Cu-Ag hybrid crystal structure, where central axis of both Cu NW and Ag NP is [110] direction and growing plane is along (111) facets.

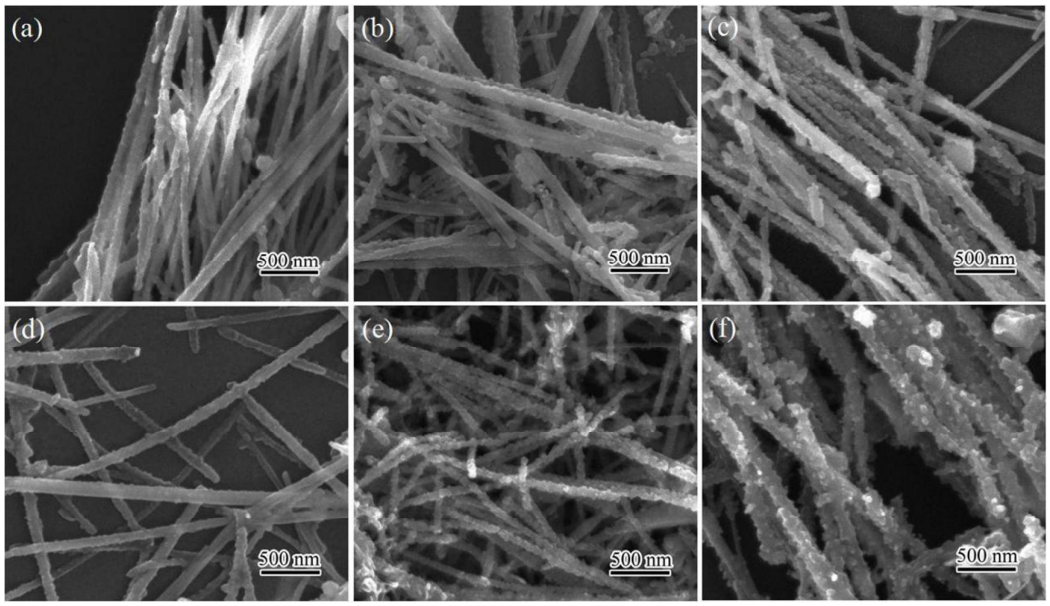

Figure 4 The growth process of Ag NPs on Cu NWs at different time in different solutions: (a) 1 min (b) 5min (c) 10min with Cu/Ag equaling to 10:1; (d) 1 min (e) 5min (f) 10min with Cu/Ag equaling to 5:1.

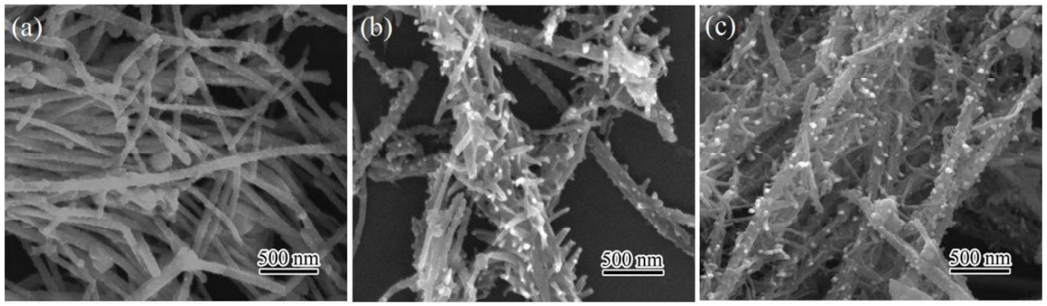

Figure 5 The growth process of Ag nanostructures on Cu NWs at different time when the ratio of Cu to Ag equals to 1:1: (a) 1 min (b) 5min (c) 10min.

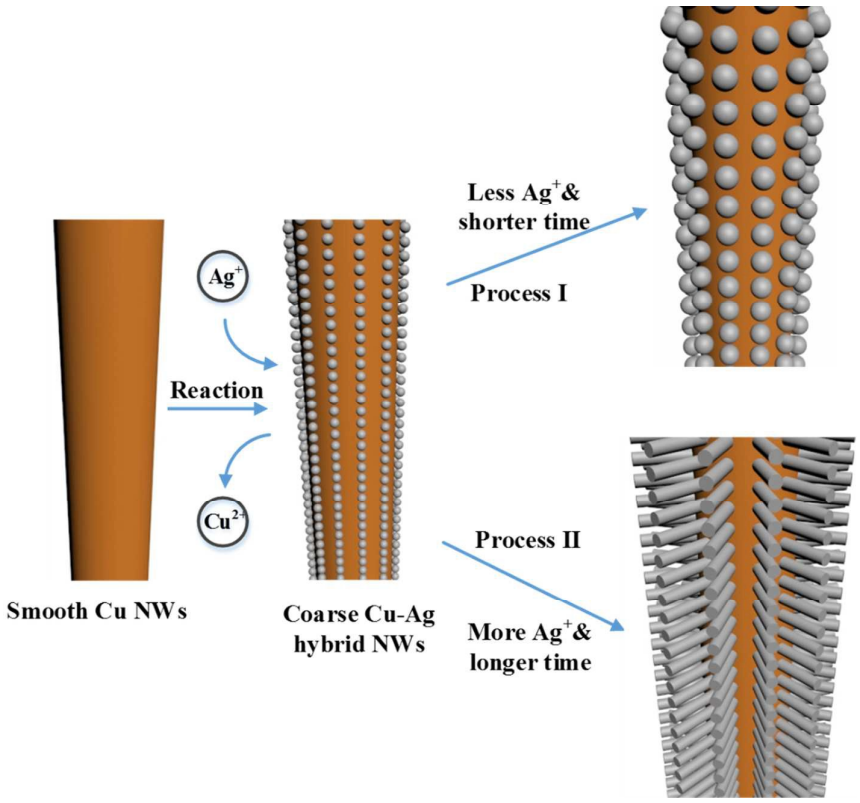

Figure 6 The schematic diagram for the growth mechanism of the Ag nanostructures on the surfaces of Cu NWs .

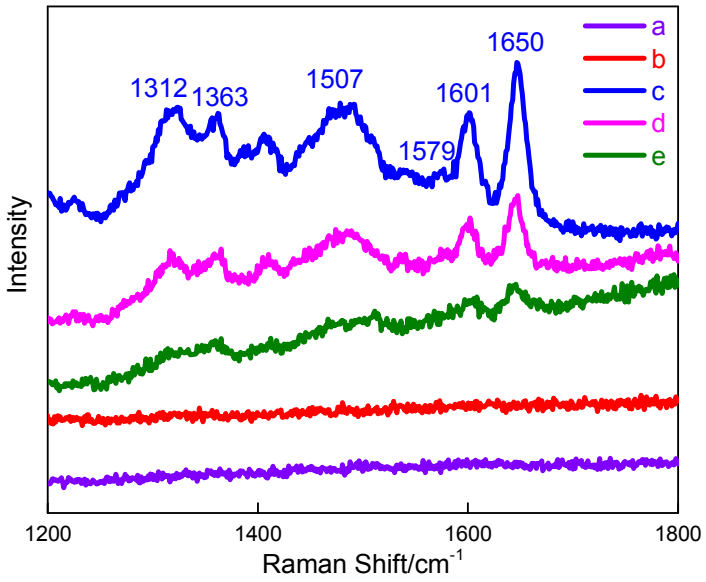

Figure 7 SERS spectra of R6G (a) with a concentration of 10^{-2} mol·L^{-1} on bare silicon substrate and (b) with a concentration of 10^{-6} mol·L^{-1} on silicon substrate covered by Cu NWs, and (c-e) with a concentration of 10^{-6}, 10^{-7}, and 10^{-8} mol·L^{-1}, respectively, on silicon substrate covered by Cu-Ag hybrid NWs

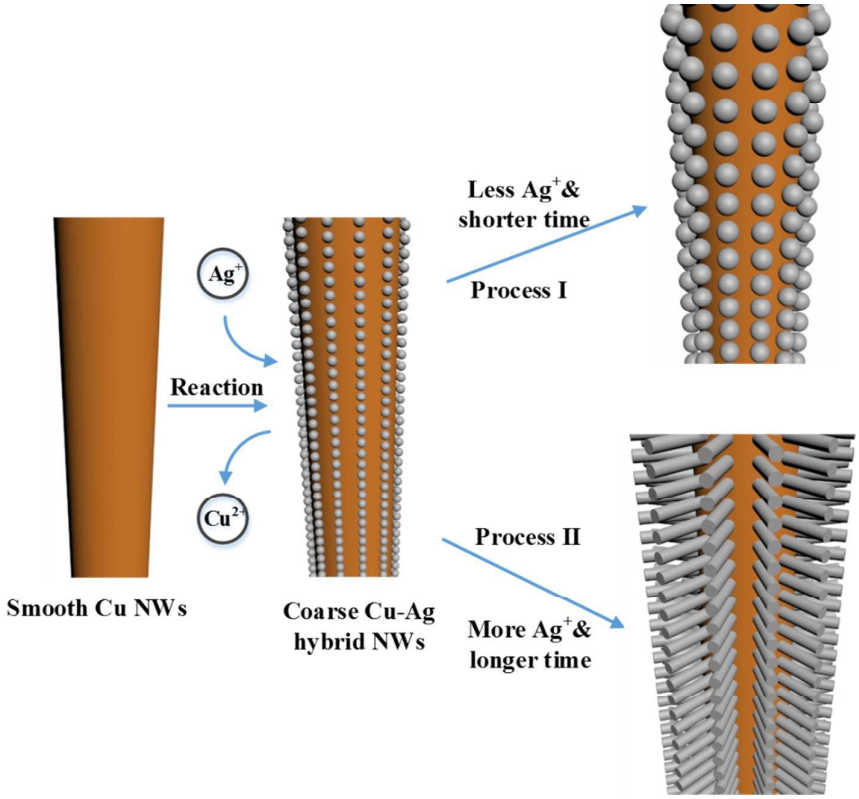

The growth mechanism and regularity of Ag-Cu hybrid nanowires synthesized by a simple solution method have be analyzed.